Reproduction, 2026, **171**(3), xaag023
https://doi.org/10.1093/reprod/xaag023
Published: 13 February 2026
Research Paper

Society for Reproduction and Fertility

ICM-autonomous regulation of mouse blastocyst primitive endoderm formation by p38-MAPK is independent of cavity expansion

Martina Bohuslavová (née Stiborová)[1], Andrea Hauserová[1], Rebecca Collier[1], Joaquin Lilao-Garzón[2], Silvia Muñoz-Descalzo[2], and Alexander W. Bruce[1,*]

[1]Laboratory of Early Mammalian Developmental Biology (LEMDB), Department of Molecular Biology & Genetics, Faculty of Science, University of South Bohemia in České Budějovice, České Budějovice, Czech Republic
[2]Laboratory of Developmental Quantitative Biology and Molecular Biology of Germ Cells, University Institute of Biomedical and Health Research, University of Las Palmas de Gran Canaria, Las Palmas de Gran Canaria, Spain
*Corresponding author: Alexander W. Bruce, Laboratory of Early Mammalian Developmental Biology (LEMDB), Department of Molecular Biology & Genetics, Faculty of Science, University of South Bohemia in České Budějovice, Branišovská 31, České Budějovice, 37005, Czech Republic. Email: awbruce@prf.jcu.cz
M.B. (née Stiborová) and A.H. contributed equally.

Abstract

Abstract: During early mouse blastocyst ICM maturation, we previously described that pharmacological inhibition of p38 mitogen-activated-kinase (p38-MAPKi) significantly impairs primitive endoderm (PrE) differentiation from an initially uncommitted population of inner cell mass (ICM) cells but does not affect pluripotent epiblast (EPI) specification. A recent report details a positive role for blastocyst cavity expansion in assisting ICM lineage formation and marker gene expression. As p38-MAPKi also results in smaller cavity volumes, we addressed to what extent p38-MAPKi-mediated impaired PrE differentiation is driven by ICM autonomous or cavity expansion mechanisms. We compared ICM differentiation phenotypes associated with either chemically inhibited cavity volume expansion or p38-MAPKi on individual cell and ICM lineage population levels. Whilst recapitulating previously observed decreases in expression of both EPI and PrE markers, we discovered that cavity expansion phenotypes are manifested in impaired numbers of specified EPI and increased numbers of uncommitted cells, rather than impaired PrE differentiation, as observed after p38-MAPKi. Moreover, using both 2D ES-cell and 3D ICM organoid models, we show PrE differentiation is also significantly impaired by p38-MAPKi in the absence of a blastocyst cavity; a result recapitulated in cultured immuno-surgically (IS) isolated early blastocyst ICMs, in which an outer PrE and inner EPI population are ordinarily formed. These data confirm that the early blastocyst requirement for p38-MAPK activity to permit PrE differentiation from uncommitted ICM progenitors is primarily ICM autonomous rather than caused by impaired cavity expansion.

Keywords ouabain, ATP1, blastocyst cavity expansion, SB220025, p38-MAPK, ICM cell-fate, epiblast, primitive endoderm, mouse ES-cell and ICM organoids

Mouse preimplantation development forms three blastocyst lineages at implantation (E4.5 - embryonic day 4.5): an outer, differentiating trophectoderm (TE) (placenta precursor; CDX2+) and two inner cell mass (ICM) lineages—the pluripotent epiblast (EPI) (foetus progenitors; NANOG+ and SOX2+) and the differentiating primitive endoderm (PrE) (a monolayer at the ICM–cavity interface contributing to yolk sac membranes; sequentially activating GATA6, SOX17, and GATA4 expression), as reviewed in (Chazaud & Yamanaka, 2016; Plusa & Piliszek, 2020). During maturation (E3.5–E4.5), we previously identified an early p38 mitogen-activated-kinase (p38-MAPK) requirement (centred around E3.5+4 to +7 hr) that permits PrE differentiation from an initially uncommitted ICM population [co-expressing NANOG and GATA6 at E3.5; (Chazaud et al., 2006)], without affecting EPI specification. This phenotype is associated with defects in ribosome-related gene expression, rRNA processing, polysome formation, and translation (Bora et al., 2019; 2021a; 2021b; Thamodaran & Bruce, 2016). p38-MAPKi is also linked to reduced blastocyst cavity expansion (Bora et al., 2021b). Cavity expansion in mice involves luminal fluid accumulation across the TE driven by ATP1 (N^+/K^+ ATPase), beginning at the 16-cell stage and coalescing into a single cavity by the 32-cell stage (E3.0–E3.5) (Motosugi et al., 2005; Ryan et al., 2019; Schliffka et al., 2024; Watson, 1992; Watson & Barcroft, 2001; Wiley, 1984).

A previous study used ouabain (OA) to inhibit ATP1 function and found that impaired blastocyst cavity expansion during maturation is associated with reduced expression of both EPI and PrE marker proteins and with impaired spatial separation of the two lineages within the ICM (Ryan et al., 2019). Building on these findings, we asked to what extent the PrE differentiation defects we previously reported under p38-MAPKi are linked to the observed

Received: September 29, 2025; **Revised:** December 22, 2025; **Accepted:** February 5, 2026

reduction in blastocyst cavity volume (Bora et al., 2021b), which could reflect compromised TE function, or whether they arise from autonomous ICM mechanisms.

After confirming impaired blastocyst cavity volume expansion with OA, we observed a concomitant and consistent reduction in the expression of EPI markers (NANOG and SOX2) and PrE markers (GATA6, SOX17, and GATA4) in ICM cells. Additionally, by the late-blastocyst stage (E4.5), OA-treated ICMs contained significantly fewer specified EPI cells than controls, while the number of specified/differentiating PrE cells was unchanged. The reduced EPI cell numbers were counterbalanced by an increased population of uncommitted ICM cells co-expressing NANOG and GATA6, indicating impaired EPI specification. These data reveal that EPI specification, rather than PrE differentiation, is more sensitive to impaired cavity expansion.

Moreover, the OA-induced phenotype differs from the inverse PrE-defect observed under p38-MAPKi conditions during the same developmental window, supporting the role of active p38-MAPK signalling in promoting PrE differentiation at the ICM level, independently of cavity expansion. Substantiating this conclusion, outer PrE cell formation in IS isolated ICMs of early blastocysts lacking TE and a cavity is impaired after p38-MAPKi; and PrE-like differentiation is also reduced after p38-MAPKi in employed 2D ES-cell and 3D ICM organoid models (Mathew et al., 2019; Schroter et al., 2015). Collectively, these findings reinforce the role of p38-MAPK signalling in PrE differentiation and highlight the distinct but interacting contributions of cavity volume expansion and ICM-autonomous mechanisms to blastocyst cell fate.

Materials and methods

Superovulation and embryo isolation

Animal work was conducted in accordance with Act No 246/1992 Coll., on the protection of cruelty against animals under the supervision of the Central Commission for Animal Welfare, approval ID 51/2015 (Czech Republic). Experimental embryos were collected as previously described (Mihajlovic et al., 2015). Briefly, F1 generations of 8-week female hybrid mice (C57BL6 female and CBA/W strain crosses) were intraperitoneally injected with 7.5 IU of pregnant mare serum gonadotrophin (PMSG; Merck) and reinjected after 48 hr with 7.5 IU human chorionic gonadotrophic hormone (hCG; Merck), before overnight mating with F1 stud males. At 4 hr before dissection, culture dishes containing 20×10 µl drops of potassium simplex optimised media supplemented with amino acids (KSOM+AA, (Embryo-Max; Millipore), covered with mineral oil (NidOil - Nidacon) and equilibrated at 37 °C in a 5% CO_2 atmosphere were prepared. For inhibitor treatments of intact blastocysts, recovered 2-cell stage embryos (E1.5; 45–47 hr post-hCG) were washed through 20 µl drops of prewarmed (37 °C) M2 media (EMD Millipore Corp. 3816047) containing 4 mg/ml bovine serum albumin (BSA; Merck) and then transferred through a series of prewarmed KSOM+AA culture drops and cultured in vitro to the desired stage, including exposure to control or specific inhibitor treatments (see *Embryo/IS isolated ICM inhibitor treatments*). For immuno-surgery experiments, 8-cell (E2.5) embryos were recovered and similarly cultured in KSOM+AA to the desired early-blastocyst (E3.5) stage for ICM isolation (91 or 96 hr post-hCG injection, see *Immuno-surgical ICM isolation*) and further cultured in vitro under control or inhibitor treatment conditions.

Immuno-surgical (IS) ICM isolation

A previously described protocol was adopted (Wigger et al., 2017). Briefly, early stage (E3.5) blastocysts (at a stage equivalent to 91 or 96 hr post-hCG injection), obtained from in vitro cultured embryos recovered at the 8-cell (E2.5) stage, were subject to zona pellucidae removal in prewarmed (37 °C) acid Tyrode's solution drops (Sigma-Aldrich. cat. #T1788) diluted in M2. Blastocysts were transferred to M2 medium drops for 15 min, incubated for 40 min in anti-mouse serum antibody (diluted 1:2 in M2 medium: Merck M5774) and then guinea pig complement (1:4 in prewarmed M2 medium) for 30 min, initiating complement-mediated outer TE cell lysis. ICMs were isolated by repeated pipetting in prewarmed M2 medium drops and subject to immediate fixation and immunofluorescence (IF) staining (see *Blastocyst/IS isolated ICM fixation and IF staining*) or cultured in KSOM+AA to the E4.5-equivalent developmental stage.

Embryo/IS isolated ICM inhibitor treatments

For blastocyst ouabain- (OA-) treatments, early-stage (E3.5) blastocysts (with cavities approximating half the embryonic volume) were transferred into pre-equilibrated KSOM+AA culture drops containing either 500 µM OA (Merck: O3125) or equivalent volumes of vehicle (dimethylsulfoxide/DMSO, Merck: D4540) solvent control and cultured to the mid- (E4.0) or late- (E4.5) blastocyst stages, fixed and, as necessary, IF stained (see *Blastocyst/IC isolated ICM fixation and IF staining*). Blastocyst p38-MAPKi treatments were performed as described for OA-treatment, but utilizing 20 µM SB220225 (Merck: 559396), unless otherwise stated, and equivalent volumes of DMSO control. For IS isolated ICM p38-MAPKi treatments, when assessing cytotoxicity, isolated ICMs were cultured in SB220225 containing KSOM+AA (5, 10 or 20 µM, or equivalent volumes of DMSO control) to the E4.5 equivalent stage, prior to fixation and light-microscopy, otherwise they were cultured in 5 µM SB220025 containing KSOM+AA until the E4.0 equivalent stage, before transfer to non-supplemented KSOM+AA and culture to E4.5, prior to fixation and appropriate IF staining.

Blastocyst/IS isolated ICM fixation and IF staining

Blastocyst/ICM IF staining protocols are described in (Mihajlovic et al., 2015). Briefly, blastocyst zona pellucidae were removed in prewarmed (37 °C) drops of acid Tyrode's solution diluted in M2. Blastocysts/ICMs were fixed, on 1.5% agar-coated culture dishes, in 20 µl drops of a 4% paraformaldehyde solution (Santa Cruz Biotechnology), overlaid with mineral oil, for 20 min at 37 °C. All subsequent steps were performed at room temperature unless stated. In 96-well micro-titre plates, blastocysts/ICMs were washed through three 70 µl drops of phosphate-buffered saline (PBST) with 0.15% Tween 20 (Merck), placed in 50 µl of 0.5% Triton-X100 (Merck) permeabilization solution (diluted in PBS) for 20 min, washed through three 70 µl drops of PBST and transferred to 50 µl drops of blocking 3% bovine serum albumin/BSA (Merck) in PBST for 30 min. Desired primary antibody dilutions were prepared in 3% BSA PBST solutions (in 5 µl volumes overlaid with mineral oil)

for overnight incubation at 4 °C. After 3 × 70 µl drop washes of PBST, embryos/ICMs were subject to a secondary 3% BSA block (1 hr) and transferred into 5 µl 3% BSA drops containing appropriate dilutions of fluorescently-conjugated secondary antibody and incubated in the dark at 4 °C for 3 hr. After three further 70 µl PBS-T washing steps, embryos/ICMs were DNA counter-stained using Vectashield mounting medium containing 4′,6-diamidino-2-phenylindole/DAPI (Vector labs). Primary antibodies (and dilutions) were as follows: (a) raised in rabbit: anti-GATA4 (sc-9035, Santa Cruz Biotechnology, 1:200), (b) raised in mouse: anti-SOX2 (sc-365823, Santa Cruz Biotechnology, 1:200), CDX2 (MU392A-UC; BioGenex, 1:200), (c) raised in goat: anti-SOX17 (AF1924, R&D Systems, 1:200), anti-GATA6 (AF1700, R&D Systems, 1:200), and (d) raised in rat: anti-NANOG (14-5761, Affymetrix/eBiosciences, 1:200). Secondary antibodies (and dilutions): (i) donkey anti-rabbit-Alexa-Fluor^{647} (ab150075, Abcam, 1:500), (ii) donkey anti-mouse-Alexa-Fluor^{488} (Abcam # ab150107, ThermoFisher, 1:500), (iii) donkey anti-goat-Alexa-Fluor^{555} (A214232, ThermoFisher, 1:500), and (iv) donkey anti-rat-Alexa-Fluor^{488} (A21208, ThermoFisher, 1:500).

Blastocyst/IS isolated ICM confocal microscopy and image analysis (including statistics)

IF-stained blastocysts/ICMs were imaged, using standard protocols, by fluorescence confocal microscopy as previously described (Bora et al., 2019; 2021a; 2021b; Gahurova et al., 2023; Mihajlovic et al., 2015; Mihajlovic & Bruce, 2016; Thamodaran & Bruce, 2016), ensuring identical acquisition settings for all comparative control versus experimental groups (that were also simultaneously IF stained, collectively, aiding the semi-quantitative analyses of specific marker protein-derived IF signals, which can be influenced by variables such the angle of imaging or *z*-section depth). Briefly, blastocyst/ICM samples were imaged on glass-bottomed 35 mm culture dishes (NC9341562, MatTek) in 20 µl drops of Vectashield mounting medium overlaid with mineral oil on an inverted Olympus FV10i confocal microscope. Per blastocyst/ICM, a full and non-overlapping *z*-series of confocal sections was acquired and micrograph images visualised (and prepared for figure generation) using the Olympus Fluoview ver.1.7, FIJI (Schindelin et al., 2012) or Imaris software. Per blastocyst/ICM, individual cell numbers were counted (based on DAPI-stained nuclei) and further subcategorised as outer or inner cells, and then based on their composite expression of detectable IF-stained lineage markers (see tabulated summaries in the supplementary Excel data/statistics tables in the online supplementary material). Absolute mean cell numbers, per blastocyst/ICM, for each lineage marker-expressing category were calculated as average percentage contribution to the overall ICM populations in each control and experimental condition derived (an infrequent minority of mitotic ICM cells were excluded); such absolute numbers (plus calculated mean SDs) and percentage contributions were charted using GraphPad Prism 8 or Microsoft Excel, respectively. Statistical significance of control versus experimental conditions were determined; (i) for normally or non-normally distributed absolute cell number mean data sets (determined with D'Agostino–Pearson and Anderson–Darling tests), using unpaired Student's t-tests or Mann–Whitney tests, respectively, and (ii) for average percentage ICM contribution using appropriate Z-tests or Mann–Whitney tests (or in the case of IS ICM-related data, using unpaired Student's t-tests) employing a significance threshold of $p < 0.05$ (*); see supplementary Excel data/statistics tables. Individual cell lineage nuclear marker protein IF levels, per blastocyst/IS isolated cultured ICM (from four randomly selected, blastocysts/ICMs in each quartile with respect to total blastocyst cell number), were calculated, as previously described (McCloy et al., 2014; Potapova et al., 2011), and employed (Bora et al., 2021b; Gahurova et al., 2023) as corrected total cell fluorescence (CTCF) in FIJI (Schindelin et al., 2012), from minimal composite confocal micrograph *z*-sections (encompassing the entire nucleus). Individual measurements were set using the FIJI command Analyze>Set Measurements, and the following options selected: area, mean grey value and, integrated density. Using the Polygon selection tool, an area encompassing individual cell nuclei was demarcated and measurements recorded. The selected area was translocated to encompass an area excluding the embryo for normalizing background measurements. From repetitive tabulated data, the CTCF, in arbitrary units, was determined for each nucleus as follows: CTCF = integrated density – (area of selected cell × mean fluorescence of background readings). Calculated CTCFs were plotted as scatterplots, indicating means and standard deviations/SDs (GraphPad Prism 8) and mean CTCF differences statistically tested via Mann–Whitney tests or unpaired Students's t-tests after confirmation of normally distributed data (D'Agostino–Pearson and Anderson–Darling tests); significance threshold $p < 0.05$ (*); see supplementary Excel data/stats tables.

Blastocyst cavity volume calculations

For OA- and SB220225-treated (plus corresponding DMSO controls) fixed blastocyst groups, the pico-litre (pl) volume of derived cavities was determined in FIJI [ImageJ (Schindelin et al., 2012)] by measuring the outer circumference of the cavity in the centrally located widest Z-stack (with the following settings: Analyze>Set Measurements; and selecting the Perimeter option; using the Polygon selection tool to trace and measure the inner cavity circumference). The radii of measured circumferences were deduced and used to calculate an approximate equatorial sectional area from which a pl value could be mathematically determined. SDs were calculated, and observed differences in the experimental/control cohorts were statistically tested (after assessing the normal or non-normal distribution of the data with D'Agostino–Pearson and Anderson–Darling tests) by using unpaired Student's t-tests or Mann–Whitney tests, respectively (*$p < 0.05$); see supplementary Excel data/stats tables.

2D mouse embryonic stem-cell (ES-cell) and 3D ICM organoid model cultures and p38-MAPKi

Mouse ES-cells (*Tet::*GATA6mCherry) were maintained on 0.1% gelatine-coated tissue culture dishes in Glasgow's minimum essential medium/GMEM-based medium supplemented with 10% foetal bovine serum/FBS, sodium pyruvate, 50 µM β-mercaptoethanol, glutamax, non-essential amino acids, and leukaemia inhibitory factor (LIF), and incubated at 37 °C and 5% CO_2. To model ICM specification into EPI-like and PrE-like cells,

2D cultures of *Tet::*GATA6mCherry mouse ES-cells (Schroter et al., 2015), or derived 3D ICM organoids (Mathew et al., 2019), were employed as described. For the 2D model, differentiation was induced by adding 500 ng/ml doxycycline/DOX to the culture medium for 6 hr, followed by further culture in serum + Leukemia Inhibitory Factor/LIF for an additional 24 hr (in the absence of DOX). 3D ICM organoids were generated by a similar 6-hr induction in DOX-containing medium, after which 50 ES-cells were seeded in coated (1% low-melt agarose in PBS) concave wells of 96-well plates in medium containing serum + LIF (briefly pulse centrifuged) and cultured for 48 hr (until aggregate ICM organoids formed). p38-MAPK inhibitor SB220025 at 5, 10, or 20 µM (or equivalent volumes of DMSO control) was added during the +DOX induction phase for 6 hr (+DOX). IF staining was performed as previously described (Kalmar et al., 2009). Briefly, adhered cells or ICM organoids were rinsed in borate buffer solution/BBS-$CaCl_2$ prior to fixation in 4% paraformaldehyde for 15 min at room temperature and three washes in BBS-BSA (0.1% Triton X-100, 0.5% BSA) permeabilisation/blocking solution for 15 min. Cells were incubated in primary antibody overnight at 4 °C in a humidity chamber. Primary antibodies included: NANOG (14-5761-80, eBIOSCIENCE, 1:200), GATA6 (AF1700, R&D Systems, 1:200), GATA4 (sc-9053, Santa Cruz Biotechnology, 1:200). Cells were then washed three times with BBS-BSA for 15 min before incubation in appropriate secondary antibody for 1–3 hr in the dark; (i) donkey anti-rat Alexa-Fluor^{488} (A-21208, ThermoFisher, 1:1000), (ii) donkey anti-goat Alexa-Fluor^{568} (A-11057, ThermoFisher, 1:1000), (iii) donkey anti-rabbit Alexa-Fluor^{647} (A-31573, ThermoFisher, 1:1000). Nuclei were visualized via DAPI counter-staining (D1306, ThermoFisher, 1:1000 in PBS). Cells were then washed three times (10 min) in BBS-$CaCl_2$ and mounted using prepared mounting medium (high mounting medium; 4% *N*-propyl-galate, 80% glycerol).

2D mouse ES cell and 3D ICM organoid model microscopy and image analysis

Cells were imaged using an inverted Zeiss LSM Zeiss LSM700 and a Plan-Apochromat 40x/1.3 Oil differential interference contrast/DIC (ultra-violet/UV) VIS-IR M27 objective. Images were acquired using 512 × 512 pixels (159.73 × 159.73 µm) resolution of specimens that were simultaneously IF stained under identical conditions and imaged under identical conditions regarding laser intensity, gain, and pinhole aperture during a single confocal session. Zeiss AIM software (Carl Zeiss Microsystems) and FIJI (Schindelin et al., 2012) were used for image acquisition and visualisation, respectively. Cell images were processed and analysed as previously described (Fischer et al., 2020). Briefly, a Matlab-based software called Modular Interactive Nuclear Segmentation (MINS) was used to segment ES-cell confocal images based on the DAPI nuclear stain (Lou et al., 2014). MINS detected and segmented each nucleus, providing a fluorescence intensity output of each channel of each individual cell. Composite analyses were performed, using the software Paleontological Statistics (PAST; https://palaeo-electronica.org/2001_1/past/issue1_01.htm), of NANOG, GATA6, and GATA4 fluorescence levels to permit the calculation of threshold levels by which individual cells were classified as positive or negative for each protein marker.

2D mouse ES cell and 3D ICM organoid model statistics

Analysis of Variance/ANOVA with Tukey's multiple comparison tests were used for comparisons between groups and Z-tests for frequencies, followed by Bonferroni correction for multiple comparisons. Values of $p < 0.05$ (*) were considered statistically significant. Statistical tests were performed using GraphPad Prism version 8.0.0 for Windows, GraphPad Software, San Diego, CA, USA (www.graphpad.com).

Results

OA and p38-MAPKi-induced blastocyst cavity expansion defects result in distinct ICM cell fate population phenotypes

We previously reported that cultured mouse blastocysts (E3.5-E4.5) exposed to p38-MAPKi [using SB220025 (Jackson et al., 1998)] show more uncommitted ICM cells (NANOG+ and GATA6+) and fewer differentiating PrE cells (GATA4+), with little effect on EPI specification (NANOG+ but lacking GATA6/GATA4), indicating impaired PrE progenitor differentiation (Thamodaran & Bruce, 2016). Additionally, p38-MAPKi–treated blastocysts have significantly reduced cavity volume (Bora et al., 2021b). Another study shows that experimentally reducing cavity expansion (via OA-mediated ATP1 inhibition or cavity-fluid removal) lowers expression of EPI and PrE marker proteins (SOX2 and GATA4) and impairs ICM cell sorting (Ryan et al., 2019); directly implicating an inductive cell-signalling role for cavity-deposited FGF4 and invoking potential physical/mechanosensory-based mechanisms, based on dynamic changes in cell adhesion and shape and altered gene expression, as inferred from studies of tissue morphogenesis throughout development (reviewed in Mammoto et al., 2013). Therefore, we aimed to extend these findings and determine how OA treatment affects the derivation and final EPI versus PrE composition of the late-blastocyst (E4.5) ICM lineages. We also sought to compare OA-phenotypes with those of p38-MAPKi during the same maturation window to understand whether p38-MAPKi-mediated impairment of PrE specification/differentiation arises from cavity expansion effects per se or from ICM-autonomous mechanisms.

We first recapitulated our published p38-MAPKi blastocyst maturation phenotypes (E3.5–E4.5), showing impaired PrE specification/differentiation and reduced cavity volume expansion (Bora et al., 2021b; Thamodaran & Bruce, 2016), assessed by IF staining for GATA4/GATA6 and NANOG or GATA4/GATA6 and SOX2 (supplementary Figures S1 and S2, see online supplementary material; assaying ICM cell fate resolution, quantified marker protein fluorescence levels, and blastocyst cavity volume). Following an analogous approach, we cultured early blastocysts (E3.5) in the presence of OA (as previously described by Ryan et al., 2019) or dimethylsulfoxide (DMSO) vehicle control for 12 hr (E4.0) or 24 hr (E4.5). Consistent with previous reports (Bagnat et al., 2007; Manejwala et al., 1989), OA treatment caused significant cavity-volume defects and by E4.5 was associated with impaired blastocyst hatching [i.e., 26/28 (93%) in DMSO versus 2/32 (6%) after OA-treatment; with an observed rate of 2/11 (18%) after a

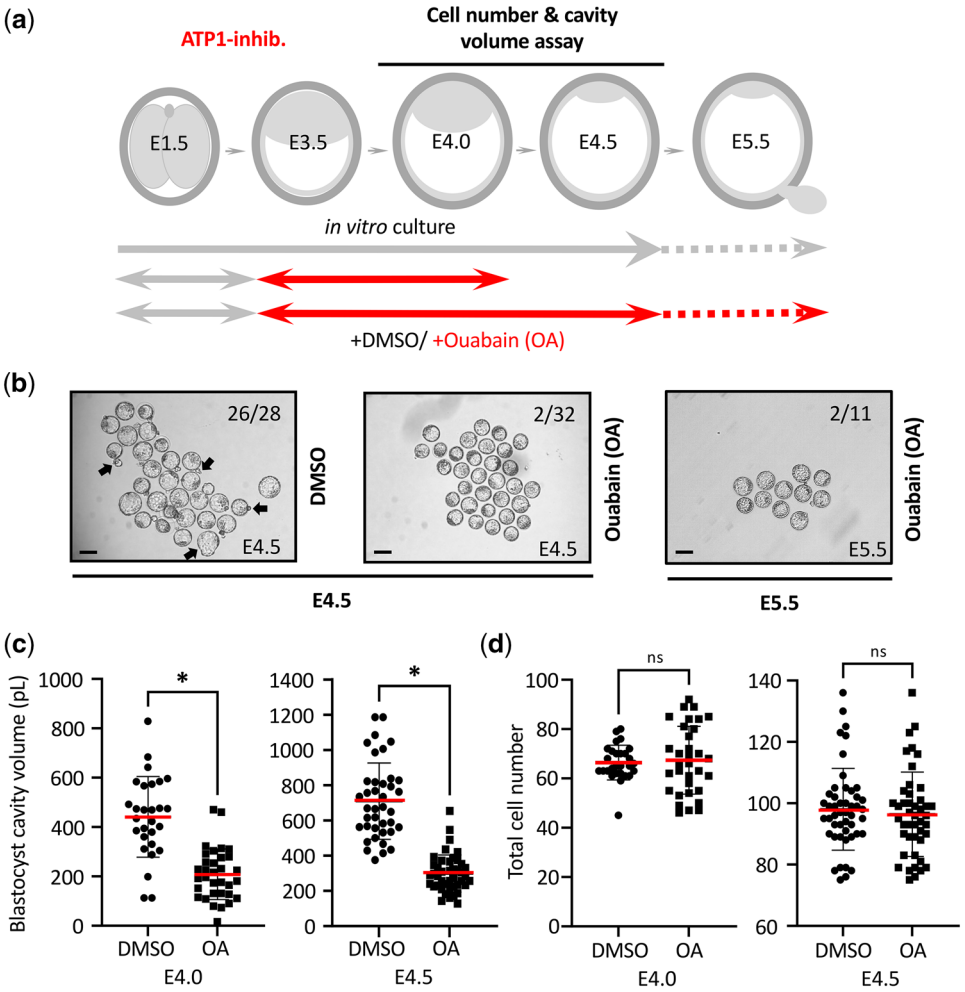

Figure 1 Ouabain (OA) treatment during blastocyst maturation causes reduced cavity size and impaired hatching without affecting total embryo cell number: (a) Experimental scheme of OA treatment and assay points, for total embryo cell number and blastocyst cavity volume, during blastocyst maturation period (E3.5–E4.5); note, an OA-treated group of blastocysts was cultured for a further 24 hr (E5.5) to observe incidences of hatching. (b) Bright-field micrographs of control [dimethylsulfoxide (DMSO)] or OA-treated blastocyst groups at E4.5 (left); note impaired blastocyst hatching (see arrows in control) after OA treatment, which persisted to the equivalent E5.5 stage (right); the number of hatching, over total, blastocysts cultured per treatment group is indicated; scale bar 100 µm. (c) Average blastocyst cavity volume per control or OA-treated blastocyst group at E4.0 (left) or E4.5 (right). (d) Average total cell number per control (DMSO) or OA-treated blastocyst group at E4.0 (left) or E4.5 (right). (c) and (d): arithmetic means (red bars), SDs and statistically significant differences are highlighted (for normal or non-normally distributed data, unpaired t-test or Mann-Whitney tests were employed, respectively. $*p < 0.05$; see supplementary data/stats Excel tables).

further 24 hr of culture in OA], without affecting total embryo or ICM cell numbers at either time point (Figure 1).

To extend these findings, we conducted confocal microscopy IF imaging to quantify: (i) ICM population sizes of specified EPI, differentiating PrE, and uncommitted progenitors (unique to this study), and (ii) the detected IF levels of ICM lineage markers (as conducted in Ryan et al., 2019). This served two purposes. Firstly, to corroborate and expand the OA-related ICM cell-fate data, and secondly, to provide an OA-related reference dataset for comparing phenotypes with those induced by p38-MAPKi. Furthermore, to broaden the repertoire of lineage markers and developmental timepoints analysed under OA-treatment conditions, we probed combinations of EPI markers (NANOG or SOX2) with PrE markers (GATA6, SOX17, or GATA4) following OA treatment. Under ±OA conditions, we first determined the average number of cells contributing to ICM sub-populations at E4.0, based on assigning combinations of expressed lineage markers: NANOG, GATA6, and GATA4. These are summarised as population percentage contributions across the whole ICM (Figure 2 and Figure S3, see online supplementary material) or as absolute cell numbers per embryo (Figure S4, see online supplementary material), with associated analyses of detected IF levels for each marker (Figure S5, see online supplementary material) as a semi-quantitative readout of marker protein expression. At E4.0, many ICM cells in both control (DMSO) and OA-treated blastocysts remained NANOG+ and GATA6+ (N+G6+), i.e., uncommitted progenitors, indicating incomplete resolution of EPI- and PrE-specified progenitors by this stage (orange arrows in Figure 2b). However, OA-treatment significantly increased the percentage of uncommitted ICM cells compared with DMSO (57.0% versus 47.0%, Figure 2c) and reduced the fraction of EPI-specified cells (N+G6−) from 20.2% in DMSO to 14.4% in OA. The proportion of PrE-specifying cells (N−G6+G4−) showed

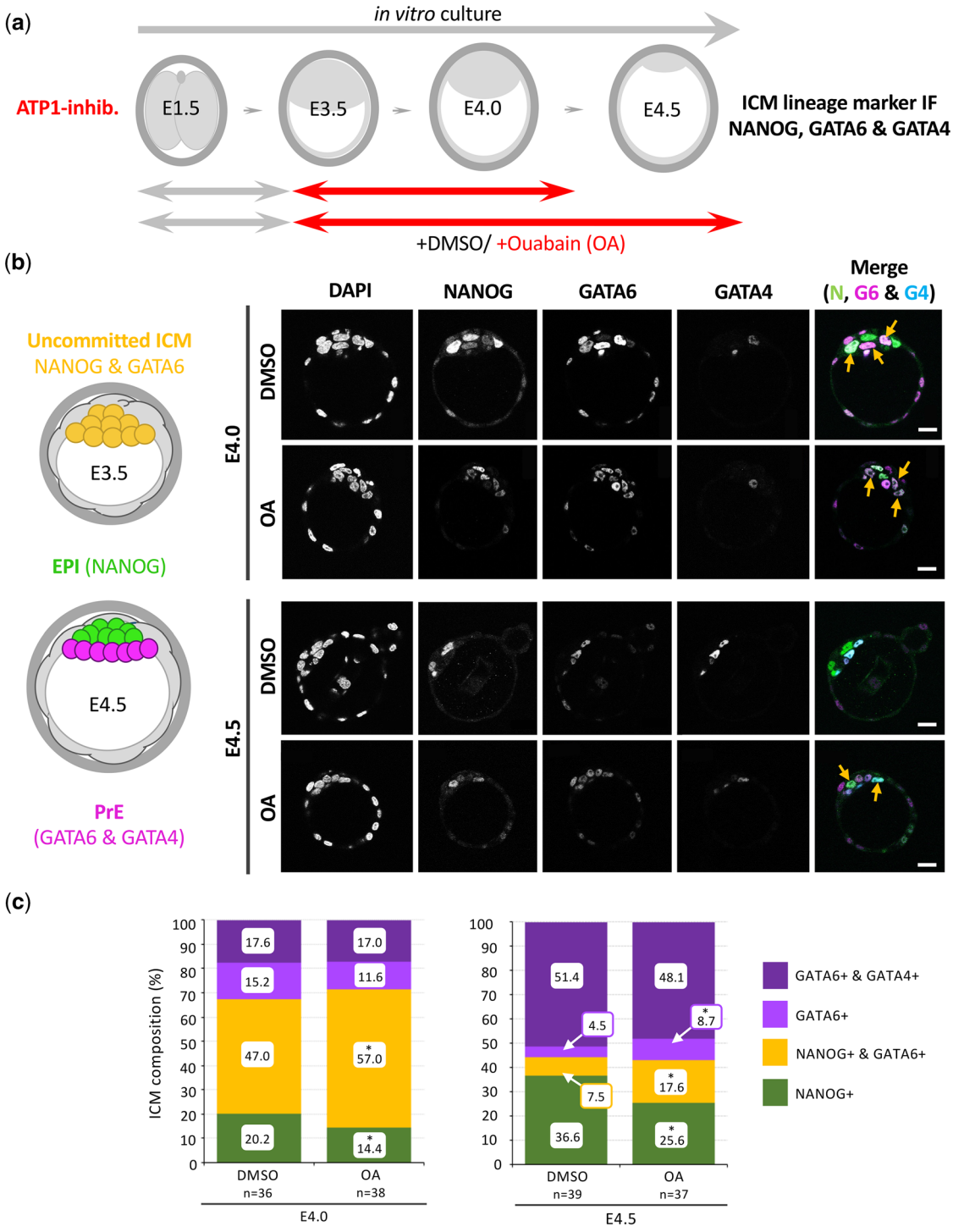

Figure 2 Ouabain treatment during blastocyst maturation impairs EPI specification from uncommitted ICM progenitors without affecting PrE differentiation (IF: NANOG, GATA6, anda GATA4): (a) Experimental scheme of OA treatment and assay points during blastocyst maturation period (E3.5–E4.5). (b) Left: schematic diagram of typical expression of ICM lineage marker proteins in uncommitted early-blastocyst (E3.5) stage (NANOG and GATA6 co-expression, yellow) and at the late-blastocyst (E4.5) stage (EPI NANOG alone, green, PrE GATA6 and GATA4 in the absence of NANOG, magenta). Right: example confocal single *z*-section micrographs of control [dimethylsulfoxide (DMSO)] or OA-treated blastocysts IF assayed for combined NANOG, GATA6, and & GATA4 expression at E4.0 and E4.5 (scale bar, 20 µm). (c) Average cellular percentage ICM composition of control (DMSO) or OA-treated blastocysts IF assayed for cell lineage marker expression at E4.0 and E4.5; delineated as uncommitted (co-expressing NANOG & GATA6, orange), PrE (expressing GATA6 alone, light purple, or GATA6 plus GATA4 without NANOG, dark purple), and EPI (expressing NANOG without GATA6 or GATA4, green); note, no cells express GATA4 alone, in the absence of either of the other assayed markers. Statistically significant differences highlighted (Z-test; $*p < 0.05$, see supplementary data/stats Excel tables; embryo *n*-numbers highlighted). See Figure S3 for the same data represented as pairwise comparisons of NANOG and GATA6 or NANOG and GATA4 (co-)expression, and Figure S4 for average total cell number data per assayed embryo. Note, OA-treatment results in unaffected PrE specification, impaired EPI formation, and increased incidence of uncommitted ICM cells (at E4.0 and E4.5), versus the control DMSO-treatment; see orange arrows in (b).

a non-significant difference between groups (DMSO 15.2% versus OA 11.6%, Figure 2c). The fraction of ICM cells expressing the later PrE marker GATA4 (which was always co-expressed with GATA6) was also not significantly different between groups (DMSO 17.6% versus OA 17.0%, Figure 2c). Since OA did not affect total blastocyst cell number (Figure 1), the shifts in ICM composition at E4.0 with OA are also reflected in the overall cell-number changes, with fewer EPI-specified cells (N+G6−) and more uncommitted cells (N+G6); and, PrE-specified cell numbers, marked by GATA6 in the absence of NANOG or by GATA4, did not significantly differ (Figure S4, see online supplementary material). Although OA-treatment selectively impaired EPI specification, it did not alter the average per-cell NANOG-specific IF levels within EPI (N+G6−) or uncommitted (N+G6+) cells. By contrast, GATA6 IF levels were significantly reduced in both uncommitted (N+G6+) and specifying PrE (N−G6+) cells, even though such PrE-related populations were unaffected in size. Notably, detected GATA6 fluorescence remained unchanged in those PrE cells that had already begun to express GATA4 (N−G6+G4+), and GATA4 fluorescence levels themselves were unchanged (Figure S5, see online supplementary material). Taken together, OA-induced cavity-size reduction at E4.0 correlates with impaired EPI progenitor specification from the initially uncommitted E3.5 ICM, without altering average NANOG fluorescence levels in those cells, but it does not impair PrE specification/differentiation, even though GATA6 fluorescence is reduced in some uncommitted and early PrE subpopulations that have not yet expressed detectable GATA4.

We next asked what effect OA treatment would have on E4.5 stage blastocyst ICMs (Figure 2c and Figures S3 and S4). A smaller population of uncommitted ICM progenitors (N+/G6+) remained observable in both DMSO- and OA-treated embryos, reflecting ongoing ICM fate resolution during later blastocyst maturation. However, as at E4.0, this uncommitted population was significantly greater with OA treatment than in control DMSO conditions (7.5% in DMSO versus 17.6% in OA of the total ICM). Similarly, there was a significant reduction in the proportion of specified EPI cells (N+/G6−) in OA-treated embryos (DMSO 36.6% versus OA 25.6%), while the overall contribution of PrE-specified cells (N−G6+G4- plus N−G6+G4+ populations) did not significantly differ between groups (DMSO 55.9% versus OA 56.8%); although, there was a small, yet significant, increase in PrE-specified cells that only expressed GATA6 in the absence of GATA4 (DMSO 4.5% versus OA 8.7%; Figure 2c and Figure S3). Thus, OA treatment throughout the entire blastocyst maturation period, which also impairs cavity expansion (Figure 1), uniquely disrupts the specification of EPI progenitors from initially uncommitted ICM cells, while overall PrE specification is not similarly affected (these phenotypes are also evident when looking at the averaged total ICM cell numbers at E4.5, Figure S4). This indicates that the mid-blastocyst (E4.0) specification defects persist through to the late-blastocyst stage. Although even in the continued presence of OA, the ICM percentage contribution of EPI-specified cells (only expressing NANOG) did increase (i.e., from 14.4% at E4.0 to 25.6% at E4.5, Figure 2 and Figures S3 and S4), indicating that EPI-specification was not blocked but merely delayed. An analysis of the average IF levels of all three lineage markers showed that OA treatment significantly reduced detectable NANOG levels in both EPI-specified cells (N+G6−) and uncommitted cells (N+G6+). GATA6 and GATA4 IF levels were also reduced in PrE-specified and differentiating cells (i.e., N−G6+ and N−G6+G4+), but GATA6 fluorescence in uncommitted cells (N+G6+) remained unaffected (Figure S5). These findings align with previous reports that OA treatment diminishes detectable EPI (SOX2) and PrE (GATA4) marker expression up to E4.0, even though those earlier studies examined blastocysts flushed at E3.5 (Ryan et al., 2019) rather than those cultured from the 2-cell stage.

We repeated both OA treatment regimens and assayed SOX2 (as in Ryan et al., 2019) and SOX17 expression as alternative markers for the EPI [SOX2 (Avilion et al., 2003; Wicklow et al., 2014)] and PrE [SOX17 (Artus et al., 2011; Niakan et al., 2010)] lineages (Figure 3 and Figure S6, see online supplementary material). At E4.0, OA caused a significant reduction in the proportion of EPI-specified cells that express only SOX2 (S2+S17−; DMSO 51.1% versus OA 38.9%), while the proportion of PrE-specified cells (S2−S17+) did not differ significantly (DMSO 20.3% versus OA 16.4%). OA also led to a significantly higher fraction of ICM cells co-expressing both markers (S2+S17+; DMSO 28.6% versus OA 44.7%). These trends were mirrored in the averaged total ICM cell numbers (Figure S6). Interestingly, despite SOX17 being a temporally later PrE marker than GATA6 (in the absence of NANOG), a large proportion of mid-blastocyst (E4.0) ICM cells, even in control DMSO conditions, initiated SOX17 expression while SOX2 remained present. Moreover, such co-expression of SOX2 and SOX17 was further enhanced by OA treatment. Although SOX2/SOX17 co-expression resembles uncommitted cells co-expressing NANOG/GATA6 (i.e., co-expression of respective EPI and PrE markers), it may be more appropriate to interpret this state as a transient phase of ICM specification, arising during the transition from the early-blastocyst stage, rather than a maintained condition, given that early-stage (E3.5) blastocyst ICM cells co-express NANOG and GATA6 but do not express SOX17 (Chazaud et al., 2006; Niakan et al., 2010; Thamodaran & Bruce, 2016). Furthermore, whilst ICM cells of maturing blastocysts ordinarily transit this state, as evidenced in the DMSO-treated control group, it is potentiated by OA treatment and its associated cavity volume expansion defects (Figure 1), and it is marked by enhanced SOX2, yet unchanged SOX17, levels of IF (Figure S7, see online supplementary material). Despite this, when OA treatment was applied from E3.5 to E4.5, the percentage compositions of ICM cells defined by SOX2 and SOX17 expression/co-expression were not statistically different (Figure 3). This resolution of ICM cell fate contrasts with the results of the NANOG/GATA6 analysis, where EPI specification from uncommitted ICM progenitors is significantly impaired at E4.0 and persists through E4.5, albeit in a manner indicative of delayed, rather than blocked specification (Figure 2 and Figures S3 and S4). Thus, the observed E4.5-related discrepancies in EPI specification when assaying NANOG and SOX2 markers may reflect differential cell-signalling and/or mechanosensory regulation of their individual expression, across the ICM, as a response to impaired cavity expansion (Figure 1). Equally, they also support the conclusion that OA-induced reductions in blastocyst cavity volume impair, rather than completely block, EPI specification. The degree of such observable impairment varies depending on the EPI markers assessed. Notably, by E4.5, the per-ICM-cell fluorescence levels of both SOX2 and SOX17 (where detected) were significantly reduced across all expression/co-expression categories (Figure S7), consistent with previous data showing OA-induced reductions in EPI (SOX2) and PrE (GATA4) markers after OA treatment between

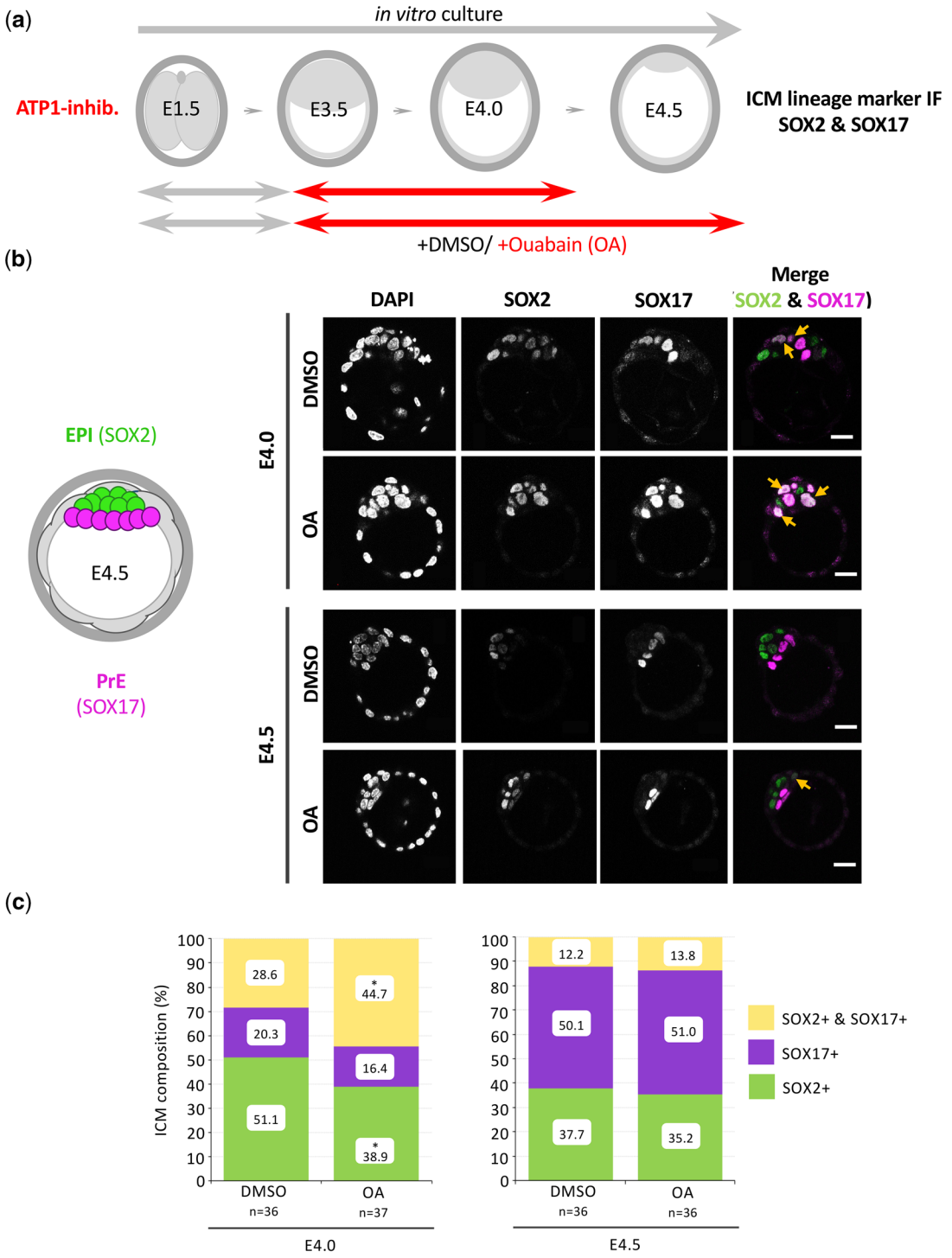

Figure 3 Ouabain (OA) treatment during blastocyst maturation impairs EPI specification without affecting PrE differentiation (IF: SOX2 and SOX17): (a) Experimental scheme of OA treatment and assay points during blastocyst maturation period (E3.5–E4.5). (b) Left: schematic diagram detailing typical expression of ICM lineage marker proteins at the late-blastocyst (E4.5) stage (EPI SOX2 alone, green, PrE SOX17, magenta). Right: example confocal single *z*-section micrographs of control [dimethylsulfoxide (DMSO)] or OA-treated blastocysts IF assayed for combined SOX2 and SOX17 expression at E4.0 and E4.5 (scale bar 20 µm). (c) Average cellular percentage ICM composition of control (DMSO) or OA-treated blastocysts at E4.0 (left) and E4.5 (right); delineated as co-expressing (SOX2 and SOX17), PrE (expressing SOX17 without SOX2), and EPI (expressing SOX2 without SOX17) cells. Statistically significant differences highlighted (Z-test; $*p < 0.05$, see supplementary data/stats Excel tables; embryo *n*-numbers highlighted). See Figure S6 for average cell number population data/per assayed embryo. Note, OA-treatment results in unaffected ICM specification of PrE at E4.0 and E4.5 and impaired formation of EPI and increased incidence of co-expressing cells at E4.0, compared to control DMSO-treatments; see orange arrows in (b).

E3.5 and E4.0 (Ryan et al., 2019). Collectively, these findings confirm that OA-mediated reductions in cavity size (Figure 1) are associated with reduced fluorescence levels of markers for both ICM lineages, but preferentially impede the differentiation of EPI progenitor cells rather than their PrE counterparts (Figures 2 and 3 and Figures S3–S7).

In summary, these analyses show that OA-induced impairment of blastocyst cavity volume expansion affects the appropriate formation of ICM subpopulations by developmentally impairing EPI specification while leaving PrE specification relatively unaffected (Figures 1–3). This is accompanied by reduced IF levels for both EPI and PrE marker proteins (Figures S5 and S7), supporting a direct cell-signalling-based and/or mechanosensory role for cavity expansion in maintaining ICM marker protein expression, as previously reported (Ryan et al., 2019). This phenotype, however, contrasts with our earlier p38-MAPKi results (Bora et al., 2019; 2021b; Thamodaran & Bruce, 2016), where PrE specification/differentiation from uncommitted ICM progenitors is compromised rather than EPI specification (Figures S1 and S2). Thus, although p38-MAPKi inhibition is associated with reduced cavity expansion, it is unlikely to be a major driver of the PrE-specific phenotype previously observed.

PrE differentiation in early blastocyst (E3.5) isolated ICMs is impaired by p38-MAPKi

To address the hypothesis that p38-MAPK supports PrE specification/differentiation via an ICM autonomous mechanism, we assayed ICM lineage formation in a context devoid of TE and associated cavity expansion, using IS isolated ICMs. Depending on exact timing, cultured IS-derived early ICMs from E3.5 mouse blastocysts, where outer TE cells are removed by complement-mediated lysis [Figure S8; (Solter & Knowles, 1975)], either reform an outer TE layer (sometimes reconstituting a cavity) or, if TE fate has already irreversibly committed (Posfai et al., 2017), develop an outer differentiated PrE encapsulating NANOG-expressing EPI cells (Wigger et al., 2017). We first reproduced these findings: ICMs isolated around 91 hr post-hCG (relative to female superovulation) and cultured for 24 hr reconstituted a TE-expressing CDX2, whereas those isolated at 96 hr formed an outer PrE layer marked by GATA4 surrounding NANOG-expressing EPI cells (Figure S8). Using the 96-hr timepoint, we identified a working concentration of 5 μM SB220025 (p38-MAPKi) that did not cause ICM cytotoxicity after 24 hr in culture (Figure S9, see online supplementary material); despite greater cytotoxic sensitivity of IS-isolated ICMs compared to p38-MAPKi in intact blastocysts, a similar 5 μM (versus 20 μM) treatment in E3.5–E4.5 cultured blastocysts still produced a small but significant increase in the proportion/number of uncommitted cells [compare Figures S10 and S11 (see online supplementary material) with previous results (Thamodaran & Bruce, 2016) or those recapitulated here in Figures S1 and S2]. The increased p38-MAPKi sensitivity of isolated ICMs most probably reflects enhanced availability of the inhibitor to ICM cells, in a context lacking overlying TE cells in blastocyst treatments.

Previously, we reported a narrow and irreversible minimal window for p38-MAPKi-mediated PrE impairment before the mid-blastocyst stage [i.e., between E3.5 and E4.0; (Bora et al., 2021b; Thamodaran & Bruce, 2016)]. This is reflected in the fact that blastocysts exposed to p38-MAPKi after E4.0 do not exhibit deficits in PrE cell numbers by E4.5, but inhibition between E3.5–E4.0, which is subsequently removed, significantly impairs PrE differentiation (Thamodaran & Bruce, 2016). Therefore, we tested the effect of 12 hr of ±p38-MAPKi (5 μM SB220025) followed by 12 hr in standard medium (to reach the equivalent E4.5 stage) on ICMs isolated at the 96-hr post-hCG timepoint, assessing EPI (SOX2) and PrE (GATA4) formation (Figure 4 and Figure S12, see online supplementary material). We found that, in accord with similar treatment of intact blastocysts (E3.5–E4.5), p38-MAPKi efficiently impaired specification and differentiation of the PrE (marked by GATA4 expression in the absence of SOX2), in stark contrast to DMSO vehicle-treated controls exhibiting a surface PrE layer. Indeed, we rarely observed cells positive for GATA4 expression in any IS-isolated ICMs after p38-MAPKi treatment (i.e., in only 3/13 ICMs assayed, comprising a total of 2.6% of all assayed cells versus 68.2% in DMSO controls), whereas all other cells expressed the EPI marker SOX2. However, we did observe that although virtually all ICM cells expressed SOX2 after p38-MAPKi treatment, the average detected per-cell SOX2 IF level was significantly reduced compared with controls (Figure S12). Consistently, this p38-MAPKi-induced reduction in SOX2 fluorescence was also seen in intact blastocysts (i.e., in cells lacking GATA6/GATA4 expression; Figure S2), although the trend did not extend to the alternative EPI marker NANOG (Figure S1), indicating differing relative stabilities in EPI lineage marker expression under p38-MAPKi conditions. Overall, we interpret these data as indicating that PrE specification and differentiation requires active p38-MAPK signalling, even in a TE- and cavity-free context, in a manner consistent with an ICM-autonomous mechanism of cell-fate resolution.

PrE differentiation in inducible 2D ES-cell and 3D ES-cell ICM organoid models is sensitive to p38-MAPKi

Previous work with the transgenic 2D mouse Embryonic Stem-(ES-) cell line *Tet::GATA6mCherry* (Mathew et al., 2019; Schroter et al., 2015) shows that a 6-hr transient exposure to doxycycline (+DOX) induces co-expression of endogenous NANOG and the recombinant, DOX-induced GATA6-mCherry protein. This co-expression mirrors the uncommitted state of early blastocyst ICM (Chazaud et al., 2006). Furthermore, after 24 hr of in vitro culture without DOX (−DOX), and even under conditions that promote ES cell pluripotency (i.e., +serum +LIF), cells adopt mutually exclusive patterns of NANOG and GATA6 expressing populations. In this model, GATA6 expression is accompanied by induced expression of other PrE markers such as SOX17 and GATA4 (Mathew et al., 2019; Schroter et al., 2015). Therefore, we adopted this ES-cell-based ICM cell fate model to test the effect of p38-MAPKi, investigating whether p38-MAPK promotes PrE fate independently of cavity-expansion-related morphologies, acting instead at the cell (and by inference the ICM) population level.

Accordingly, we exposed *Tet::GATA6mCherry* ES cells to either control DMSO or increasing concentrations of SB220025/p38-MAPKi (5, 10, and 20 μM) during the 6-hr +DOX induction period and immediately assayed for endogenous NANOG and GATA4 and recombinant GATA6-mCherry expression by

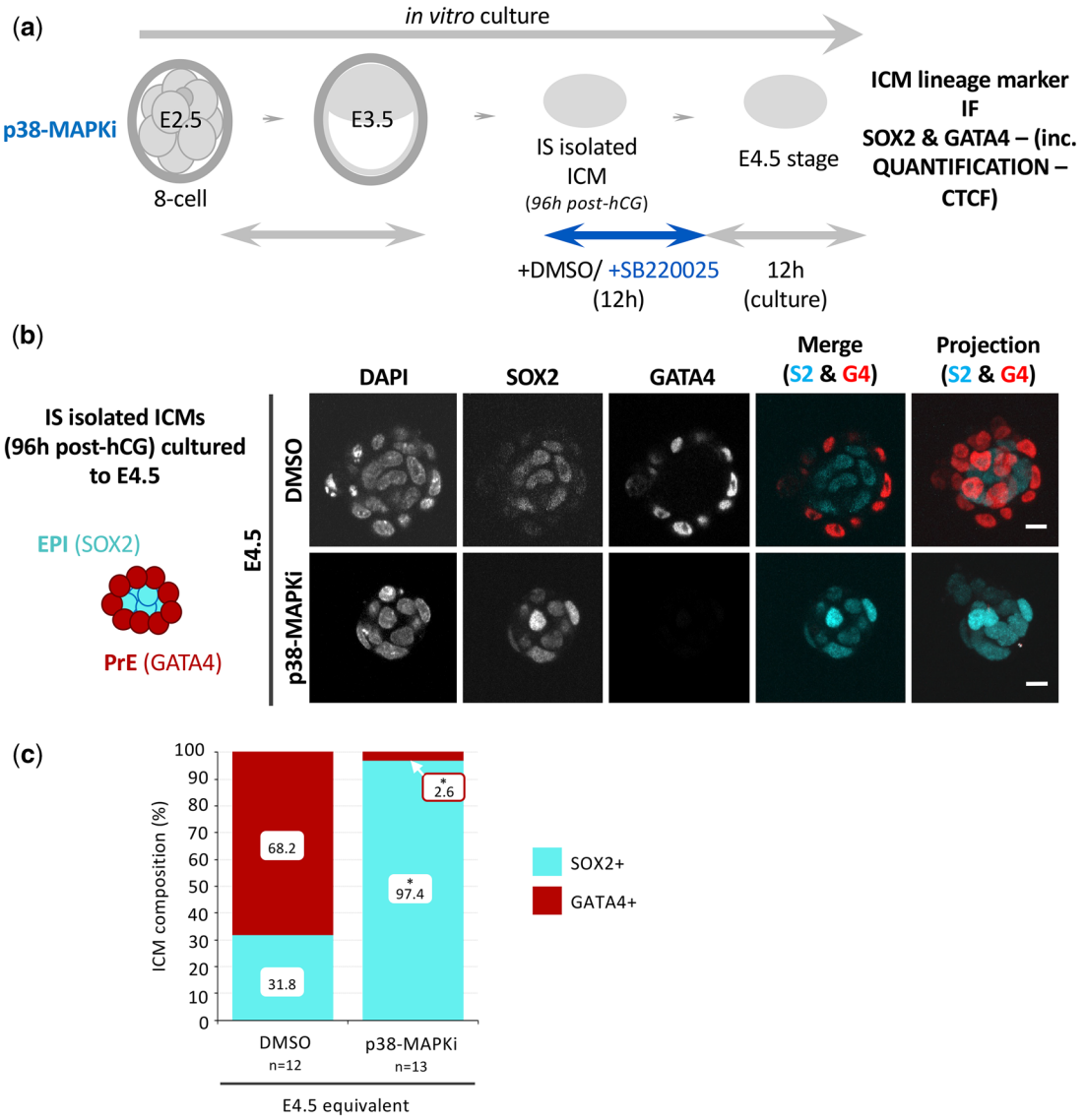

Figure 4 p38-MAPKi treatment of early-blastocyst (E3.5) stage isolated ICMs effectively impairs PrE lineage differentiation: (a) Experimental scheme of early-blastocyst (E3.5 96 hr post-human chorionic gonadotrophic hormone (hCG) superovulation microinjection) stage ICM isolation and 12-hr culture under control [dimethylsulfoxide (DMSO)] or p38-MAPKi (5 µM SB220025) conditions before transfer into regular growth medium for another 12 hrs, until the equivalent late-blastocyst (E4.5) stage, and IF staining for ICM lineage markers (SOX2 and GATA4). (b) Left: schematic diagram detailing typical expression of ICM lineage marker proteins in isolated and cultured early-blastocyst stage ICMs (i.e., after TE commitment) (EPI SOX2 alone, cyan; and PrE, red, in the absence of SOX2 expression). Right: example confocal single *z*-section micrographs of control (DMSO) or p38-MAPKi-treated ICMs IF stained for combined SOX2 and GATA4 expression (scale bar 20 µm); plus, merged images and a maximally projected *z*-section image (right-most micrographs). (c) Average cellular percentage ICM composition of control (DMSO) or p38-MAPKi-treated ICMs; delineated as EPI (SOX2) or PrE (GATA4) expressing cells. Statistically significant differences highlighted (unpaired t-test; $*p < 0.05$, see supplementary data/stats Excel tables; ICM *n*-numbers shown). See Figure S12 for average cell number population data/per assayed isolated ICM.

confocal-IF microscopy (Figures S13 and S14, see online supplementary material). Under DMSO control conditions, we confirmed co-expression of NANOG and GATA6-mCherry in the absence of detectable GATA4 (N+G6+) in 71.7% of assayed cells, resembling the uncommitted early-blastocyst ICM state and confirming successful GATA6-mCherry induction. Interestingly, 21.5% of these DMSO-treated cells showed downregulated NANOG (N−G6+), suggesting initiation of differentiation toward a PrE fate. In all p38-MAPKi treatment conditions, the proportion of such cells was significantly reduced, and the proportion of uncommitted cells (N+G6+) was significantly increased. This effect was most pronounced using 10 µM SB220025/p38-MAPKi (N+G6+ = 93.3% and N−G6+ = 2.7%), which, unlike the 20 µM treatment, did not show cytotoxicity. Additionally, quantification of the IF levels of the assayed marker proteins revealed a significantly higher NANOG-specific signal in the 10 µM p38-MAPKi-treated uncommitted (N+G6+) cells compared to DMSO controls (Figure S15, see online supplementary material), suggesting that the reduced derivation of N−G6+ cells (resembling the PrE) is antagonised by p38-MAPKi through enhanced induction of endogenous NANOG.

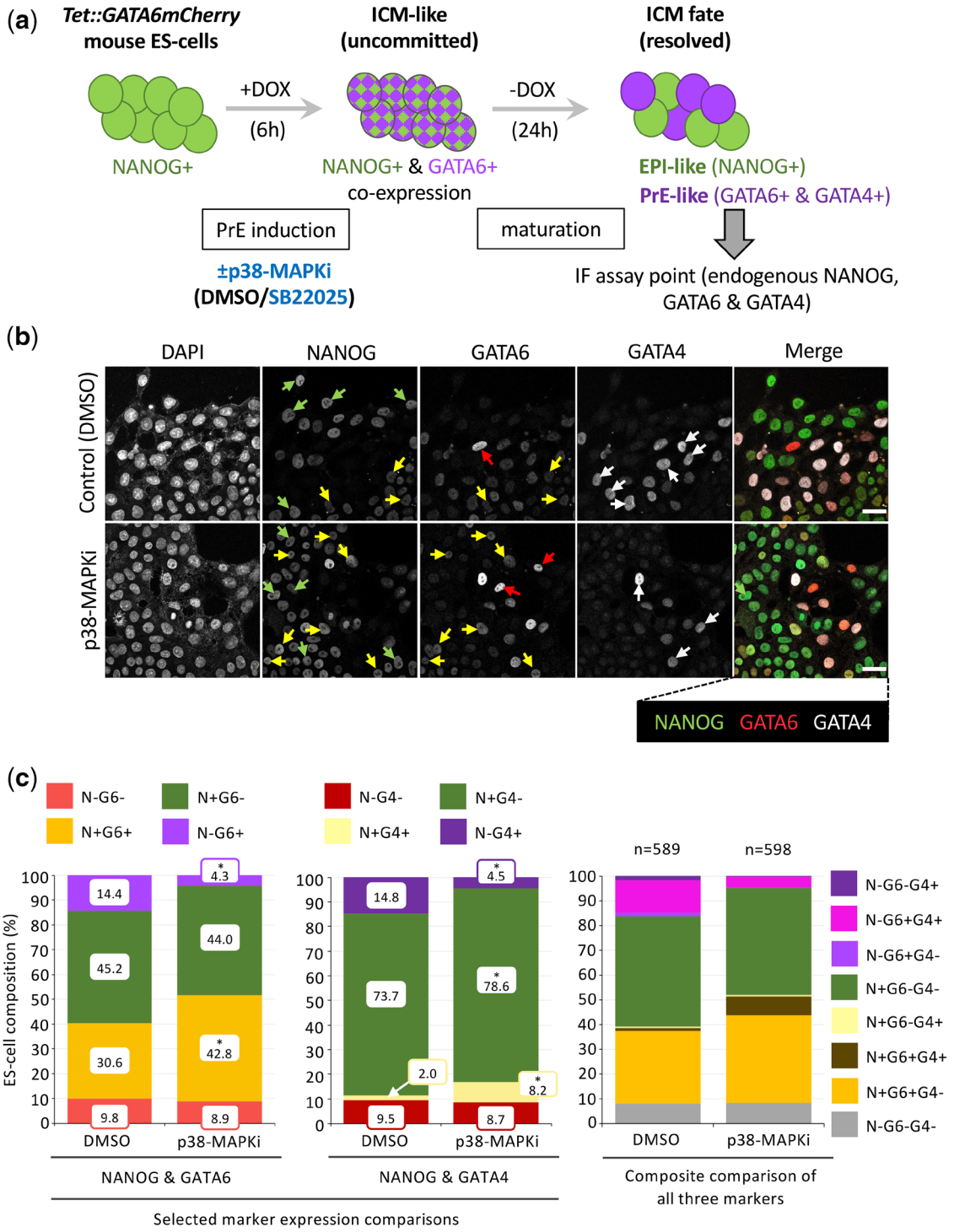

Figure 5 p38-MAPKi impairs PrE-like specification and differentiation in a 2D recombinant GATA6-inducible mouse ES-cell model: (a) Mouse ES-cell line *Tet::Gata6mCherry* is induced by a 6-hr pulse of doxycycline treatment (+DOX 6 hr) to co-express endogenous NANOG and a recombinant GATA6-mCherry. After another 24 hr of culture in regular culture media (−DOX 24 hr), individual cells mature to express NANOG or endogenous GATA6/GATA4 in a mutually exclusive pattern (Schroter et al., 2015). ES-cell cultures were exposed to +DOX 6 hr induction plus p38-MAPKi (10 µM SB220025) or vehicle control [dimethylsulfoxide (DMSO)] before transfer into regular culture −DOX 24 hr conditions for 24 hr, followed by fixation and IF-staining (NANOG, GATA6 and GATA4). (b) Example ES-cell confocal micrographs related to the indicated +DOX 6 hr treatment conditions, IF stained for endogenous NANOG, GATA6, and GATA4 (grey-scale); plus pseudo-coloured merge image (NANOG, green; GATA6, red; and GATA4; greyscale). Arrowheads denote cells exclusively expressing NANOG (green) or GATA6 (red) or those co-expressing NANOG and GATA6 (yellow) or GATA6 and GATA4 (white), respectively. Scale bars 20 µm. (c) Average cellular percentage composition of ICM cell lineage marker protein (co-)expression of indicated culture conditions, detailing: (i) compared NANOG and GATA6 (co-)expression status only (left panel), (ii) compared NANOG and GATA4 (co-)expression status only (middle panel), and (iii) all possible cell lineage marker expression combinations (right panel; +/−N = NANOG, +/−G6 = GATA6, and +/−G4 = GATA4). Individual percentage ICM contributions and statistically significant differences are highlighted (Z-test; *$p < 0.05$; total ES-cell *n*-numbers highlighted).

We next tested the effect of p38-MAPKi treatment, applied during the 6-hr +DOX induction period, on the expression of NANOG, GATA6, and GATA4, after a further 24 hr of culture in normal medium without DOX (Figure 5). Considering pairwise combinations of NANOG with either GATA6 or GATA4 expression, we found that p38-MAPKi-treated ES-cells were significantly impaired in generating cells that lack NANOG but express GATA6 (N−G6+): 14.4% in DMSO controls versus 4.3% with p38-MAPKi (Figure 5c, left panel). Similarly, cells expressing GATA4 in the absence of NANOG (N−G4+) were reduced: 14.8% in controls versus 4.5% after p38-MAPKi (Figure 5c, middle panel). This impairment was accompanied by a significant shift toward uncommitted states that co-express NANOG and GATA6 (N+G6+): 30.6% in controls versus 42.8% with p38-MAPKi. The proportion of cells expressing only NANOG without GATA6 (N+G6−) was not significantly altered (45.2% in controls versus 44.0% in p38-MAPKi; Figure 5c, left panel); however, there was a significant increase in cells expressing NANOG in the absence of GATA4 (N+G4−; Figure 5c, middle panel), indicative of a population comprising cells resembling both an EPI and uncommitted (that would also express GATA6) state, respectively. Collectively, these results follow those obtained after p38-MAPKi in intact blastocysts (Bora et al., 2019; 2021b; Thamodaran & Bruce, 2016) (recapitulated here; Figure S1) and IS-isolated ICMs (Figure 4 and Figure S12) cultured through the blastocyst maturation period (E3.5–E4.5). Unlike the timepoint immediately after +DOX induction, we did not observe a significant increase in NANOG-derived IF levels in cells in the uncommitted state (N+G6+), although GATA6 fluorescence levels were significantly elevated, including in the subset of cells that had initiated differentiation towards a state resembling the PrE (N−G6+). NANOG fluorescence levels were also significantly higher in cells reminiscent of the blastocyst EPI (N+G6− and N+G4−; Figure S16, see online supplementary material). When considering only a comparison of NANOG and GATA4 status (Figure 5c, middle panel), p38-MAPKi caused a significant increase in the proportion of otherwise uncommon cell populations co-expressing NANOG and GATA4 (N+G4+: 2.0% with DMSO versus 8.9% after p38-MAPKi), further indicating defects akin to impaired PrE differentiation in blastocysts (Figure 5, note that a comprehensive summary of all possible co-expression statuses for NANOG, GATA6 and GATA4 is provided in the right-hand chart of panel c). Collectively, these ES-cell data support a role for p38-MAPK activity in facilitating cell differentiation towards a fate resembling the blastocyst PrE.

An additional feature of the *Tet::GATA6mCherry* ES-cell system is that after recombinant GATA6-mCherry induction, cells can be driven to form 3D aggregates that, following 48 hr of culture, develop into ICM organoid structures with an outer layer, expressing GATA6, SOX17, and GATA4, surrounding an inner population that expresses the EPI marker NANOG (Mathew et al., 2019). When we formed ICM organoids from induced *Tet::GATA6mCherry* ES-cells cultured under control or p38-MAPKi conditions, we observed significant reductions in the percentage of cells expressing PrE-related markers, but not to the same extent as observed in 2D cultures: N−G6+ cell populations declined from 21.1% (DMSO) to 18.9% (p38-MAPKi) and N−G4+ declined from 21.0% (DMSO) to 18.1% (p38-MAPKi). These reductions were accompanied by modest but significant increases in cells expressing neither NANOG nor GATA6/GATA4 (N−G6−: 12.8% to 16.2%; N−G4−: 12.9% to 17.0%) (Figure S17, plus Figure S18 summarising generally reduced IF levels for all assayed marker proteins in ICM organoids derived from p38-MAPKi-treated ES-cell induction, except for NANOG in N+G4+ cells, see online supplementary material). Taken together, these data suggest that while p38-MAPKi treatment impairs differentiation from the derived uncommitted GATA6-mCherry-induced ES-cell population towards an apparent PrE fate (Figure 5 and Figures S15 and S17), the prolonged 48-hr −DOX culture required to form 3D aggregate ICM organoids provides a permissive window for partial compensatory cell-fate resolution, although the complete restoration of marker protein expression resembling blastocyst PrE differentiation observed in controls is not achieved.

Discussion

It was previously reported that OA-mediated inhibition of ATP1 during mouse blastocyst maturation (E3.5–E4.0) impairs blastocyst cavity expansion and markedly reduces expression of both EPI (SOX2) and PrE (GATA4) markers (Ryan et al., 2019). We recapitulated OA-induced cavity defects (Figure 1) and observed reductions in IF-derived fluorescence levels for an expanded set of EPI (NANOG, SOX2) and PrE (GATA6, GATA4, SOX17) markers by the late blastocyst stage (E4.5; Figures S5 and S7). However, unlike Ryan and co-workers (Ryan et al., 2019), OA treatment from E3.5 to the mid-blastocyst (E4.0) stage did not uniformly reduce such EPI- and PrE-related marker fluorescence levels, at least in cells showing mutually exclusive EPI or PrE marker protein expression patterns (Figures S5 and S7). This discrepancy may reflect our use of blastocysts cultured in vitro from the 2-cell (E1.5) stage versus freshly recovered E3.5 blastocysts (i.e., where the stated E4.0 stage may correspond more closely to a more advanced developmental stage akin to the E4.5 time-point in our data). Nonetheless, both datasets converge around our E4.5 time-point, and together support mechanotransduction or trans-cavity signalling (potentially involving luminal deposition of FGF4, as previously reported) as contributing to ICM lineage marker expression regulation (Ryan et al., 2019). Importantly, unlike the study of Ryan and colleagues, our expanded analyses, including the late E4.5 assay point and a broader panel of assayed lineage markers (notably NANOG with GATA6), reveal that OA treatment primarily impairs EPI cell specification from uncommitted ICM, while PrE populations (expressing GATA6/GATA4 without NANOG) are not similarly reduced (Figure 2 and Figures S3 and S4); a pattern opposite to the p38-MAPKi-induced PrE defects we have described (Bora et al., 2021b; Thamodaran & Bruce, 2016) and further confirmed here (again with an extended panel of lineage markers; Figures S1 and S2). It is important to note that EPI-specific phenotypes caused by ATP1 inhibition and the resulting impairment of cavity expansion most likely reflect a delayed or prolonged period of EPI specification rather than a complete block. This is supported by the observation that the proportion of EPI-specified cells (expressing NANOG alone, without any PrE marker) increases from E4.0 to E4.5 (Figure 2 and Figure S7). Our additional analysis of SOX2 and SOX17 expression reveals that OA treatment has specific effects regarding different EPI and PrE lineage markers, as by E4.5 there were no significant differences in the proportion or number of ICM cells expressing SOX2 and/or SOX17 (Figure 3 and Figure S6) compared to controls, in contrast to NANOG and GATA6 expression data (Figures 2 and Figures S3 and S4). However, exposing em-

bryos to OA until the E4.0 stage did lead to a significant increase in the proportion and number of ICM cells existing in a previously unreported state, characterised by the co-expression of SOX2 and SOX17. While this transitory state is also seen in control blastocysts, it occurs at a significantly lower frequency (Figure 3 and Figure S6). Again, these results suggest that OA treatment enhances or prolongs this transient cell fate state within the ICM. The increased frequency of SOX2 and SOX17 co-expression is associated with a reduction in the number of ICM cells expressing SOX2 alone, while the number of cells expressing only SOX17 remains unchanged (Figure 3 and Figure S6). This indicates that the enhanced transitory cell fate state caused by OA treatment primarily affects, or developmentally impedes, the specification of EPI rather than PrE progenitors. Accordingly, in EPI progenitors, OA treatment disrupts the normal resolution process by which NANOG and SOX2 cease to be co-expressed with PrE markers (GATA6 and SOX17, respectively), with this disruption being more persistent for cells expressing NANOG. This may reflect differences in the regulation or stability of GATA6 and SOX17, as by E4.5, analysis of specific IF levels shows that in cells co-expressing EPI and PrE markers, GATA6 fluorescence levels are similar to controls, but SOX17 levels are significantly reduced (Figures S5 and S7). The OA-induced increase in cells co-expressing NANOG and GATA6 likely indicates persistence of the uncommitted ICM state seen in E3.5 blastocysts (Chazaud et al., 2006), while the increased levels of SOX2 and SOX17 co-expression reflect enhanced induction of a transitory, yet typically short-lived, cell fate state. Nevertheless, both data sets indicate that blastocyst cavity expansion plays a role in ultimately facilitating appropriate EPI specification, as OA treatment delays this process, and the degree of observable delay varies depending on the EPI marker assayed (e.g., NANOG and SOX2), in combination with other recognised PrE markers. Indeed, when we examined NANOG and SOX2 (co-)expression status in response to OA treatment from E3.5 (together with GATA4 as a PrE marker), we found that by E4.25, cells co-expressing NANOG and SOX2 were reduced, indicative of a delay in EPI specification, but the proportion of ICM cells expressing SOX2 alone was increased, with near identical levels of cells expressing the PrE marker GATA4 (Figures S19 and S20); although these observed and consistent trends in EPI marker-expressing cells did not meet the threshold of statistical significance. Nevertheless, our collective findings suggest that EPI fate specification, as indicated by SOX2 expression alone, occurs earlier than that indicated by NANOG expression alone, and that such NANOG expression patterns exhibit enhanced sensitivity to OA-treatment and impaired cavity volume expansion during delayed EPI specification. Overall, our analysis of ICM cell fate in blastocysts with impaired cavity expansion shows that both EPI and PrE marker protein IF levels are ultimately and significantly reduced, consistent with previous findings (Ryan et al., 2019). Furthermore, OA treatment specifically disrupts the appropriate and timely specification of EPI cell populations, whether they arise from originally uncommitted ICM cells in the early (E3.5) blastocyst [co-expressing NANOG and GATA6 (Chazaud et al., 2006)] or from cells passing through a transitory state (co-expressing SOX2 and SOX17), while the overall specification and differentiation of PrE cells remains unaffected. Importantly, while we reference NANOG and GATA6 co-expression as indicative of an uncommitted state resembling early ICM cells (Chazaud et al., 2006), without comprehensive gene expression analysis, these cells may more appropriately be considered simply as unspecified, potentially reflecting various conflicted states arising from stochastic marker expression.

The EPI-specific ICM cell fate phenotypes associated with OA treatment are notably different from the PrE specification and differentiation defects previously observed after p38-MAPKi (Figures S1 and S2; Bora et al., 2019; Bora et al., 2021b; Thamodaran & Bruce, 2016), even though both inhibitors significantly reduce blastocyst cavity expansion (Figure 1 and Figures S1 and S2; Bora et al., 2021b). This indicates that reduced cavity expansion after p38-MAPKi is unlikely to be the main cause of impaired PrE differentiation, and supports an ICM or ICM cell-autonomous mechanism, independent of TE-derived influence. Supporting this hypothesis, we found that treating isolated ICMs from early blastocysts with p38-MAPKi, thus eliminating any influence from cavity expansion, during the critical E3.5–E4.0 period of irreversible p38-MAPKi sensitivity (Bora et al., 2021b; Thamodaran & Bruce, 2016), also leads to defective PrE specification and differentiation, while EPI specification remains unaffected (Figure 4 and Figure S12). Using established in vitro transgenic mouse ES-cell models of ICM cell fate resolution (Mathew et al., 2019; Schroter et al., 2015), we further demonstrate that p38-MAPKi treatment effectively impairs the formation of cells with marker protein expression profiles resembling the blastocyst PrE, while not affecting cells expressing markers akin to the EPI (Figure 5 and Figures S14 and S17). Notably, in the 2D culture model, 6 hr of p38-MAPKi exposure during the +DOX GATA6-mCherry induction period is sufficient to cause a significant reduction in the number of cells already initiating differentiation towards a PrE-like fate. This is accompanied by a significant increase in cells resembling the uncommitted early (E3.5) blastocyst ICM state (Figure S14). This finding accords with our previous results on intact mouse blastocysts, which revealed a brief and irreversible window of PrE sensitivity to p38-MAPKi before the mid-blastocyst (E4.0) pattern of mutually exclusive NANOG and GATA6 expression emerges (Bora et al., 2021b; Thamodaran & Bruce, 2016), strongly suggesting that p38-MAPK activity is required early in the specification process. Furthermore, when the 2D ES-cell cultures were subsequently grown in regular −DOX media (after p38-MAPKi withdrawal) the same pattern persisted (Figure 5). This model indicates that the initial 6 hr of p38-MAPKi treatment during induction is sufficient and irreversible in impairing PrE specification from uncommitted progenitors, up to at least 24 hr, reinforcing the conclusion that active p38-MAPK plays an important early role in PrE specification. Similarly, experiments testing the effect of p38-MAPKi on isolated ICMs demonstrated that early-stage inhibition, followed by a return to regular culture for 12 hr, was enough to block PrE specification and differentiation (Figure 4). In the 3D ES-cell aggregation ICM organoid model, applying p38-MAPKi during the 6-hr +DOX induction period (before cell aggregation and the unavoidably necessary 48 hr of regular culture) significantly impaired the formation of cells solely expressing the assayed PrE markers (identified by GATA6 and/or GATA4 expression without NANOG). However, this effect was less pronounced than in 2D cultures and did not result in a statistically significant increase in uncommitted cell types (co-expressing NANOG and GATA6); nevertheless, the proportion of NANOG-positive/GATA6-negative cells, reminiscent of the EPI, remained consistently unaffected (Figure S17). We speculate that the additional 24 hr of culture needed for ICM organoid formation,

in the absence of p38-MAPKi, may allow for some compensatory regulation, which could explain the weaker effect compared to the 2D model. Attempts to analyse ICM lineage marker expression after 24 hr, to detect a possible increase in potentially uncommitted PrE progenitors, were unsuccessful due to the instability of the ES-cell aggregates during fixation and staining. Notwithstanding, after 48 hr post-DOX induction with p38-MAPKi, there was a significant reduction in PrE-like cell formation and lower per cell average GATA6- and GATA4-specific IF signal (Figure S18). In intact blastocyst cultures, p38-MAPKi treatment after E3.75 or E4.0 (until E4.5) does not impair PrE specification, whereas similar inhibition of Mitogen-Activated Protein Kinase Kinases 1/2, MEK1/2 [using PD0325901, which blocks fibroblast growth facror 4/FGF4 signals promoting PrE differentiation (Yamanaka et al., 2010)] robustly blocks PrE formation (Thamodaran & Bruce, 2016). Collectively, these findings indicate that active p38-MAPK plays an important and temporally early role in blastocyst development, prior to observed ICM lineage specification, that is distinct from the later FGF4/MEK1/2-dependent mechanisms, ultimately leading to irreversible ICM cell fate decisions by the late blastocyst (E4.5) stage (Frankenberg et al., 2011; Kang et al., 2013; Nichols et al., 2009; Thamodaran & Bruce, 2016; Yamanaka et al., 2010).

We previously found that p38-MAPKi-mediated PrE phenotypes are associated with impaired general protein synthesis, reduced ribosomal protein expression, decreased polysome formation, and disrupted rRNA precursor processing. Moreover, p38-MAPKi-induced PrE defects could be partially rescued by pharmacologically activating the mammalian target of rapamycin/mTOR pathway [a key regulator of metabolism and protein synthesis (Fonseca et al., 2014)], without influencing impaired blastocyst cavity expansion (Bora et al., 2021b). This partial rescue suggested that p38-MAPK enables PrE specification and differentiation through mechanisms intrinsic to ICM cells, independent of cavity expansion, as supported by data herein. We propose that early blastocyst p38-MAPK signalling may ensure germane PrE-specification from uncommitted progenitors via ICM autonomous regulation of protein translation/synthesis, thereby priming such cells for differentiation. We recently reported that inhibition of mammalian target of rapamycin complex 1/mTORC1 during the 8- to 16-cell transition impairs the spatial allocation of daughter blastomeres to the emerging population of primary ICM founder cells, via a mechanism potentiating the 7-methyl-guanosine cap binding complex (EIF4F), which is essential for efficient translation of mRNA subclasses containing 5′ untranslated region/UTR terminal oligopyrimidine motifs; a phenotype replicated by similar p38-MAPKi treatment (Gahurova et al., 2023). p38-MAPKi effects on blastocyst PrE specification may also be related to similar impairments in selective mRNA translation, which could be investigated using embryo-optimised Scarce Sample Polysome- (SSP-) ribosomal profiling (Bora et al., 2021b; Del Llano et al., 2020; Iyyappan et al., 2023; Masek et al., 2020) or Ribo-ITP-RNAseq (Ozadam et al., 2023) to identify differential mRNA ribosome-association under ±p38-MAPKi conditions. However, p38-MAPKi-induced PrE differentiation defects are also characterized by increased numbers of uncommitted ICM cells co-expressing both GATA6 and NANOG (Figure S1; Bora et al., 2021b; Thamodaran & Bruce, 2016), suggesting that p38-MAPK activity is also required to clear putative PrE progenitors of pluripotency-associated NANOG expression, potentially through mechanisms related to protein stability. Indeed, mTORC1 inhibition from E3.5 also increases the number of cells co-expressing NANOG and GATA6, although this is associated with general developmental diapause (Bora et al., 2021b; Bulut-Karslioglu et al., 2016). This point is further supported by the observation of significant NANOG and GATA4 co-expression in p38-MAPKi-treated blastocysts exposed to concurrent mTOR activation (Bora et al., 2021b), whereby PrE specification is partially rescued but NANOG expression endures. Thus, the ICM-autonomous role of p38-MAPK in promoting PrE specification and differentiation is likely to be multi-factorial.

In summary, our findings show that OA-induced blastocyst cavity expansion leads to reduced marker protein expression in both ICM lineages but specifically impairs the specification of ICM progenitors towards the EPI lineage. This is the opposite of the effect observed after p38-MAPKi during the same developmental period, despite similar cavity expansion defects. Further, p38-MAPKi treatment of isolated ICMs and mouse ES-cell models consistently impairs PrE cell differentiation, while EPI lineages remain largely unaffected. Together, these results highlight an ICM-autonomous role for active p38-MAPK in priming PrE specification and differentiation during early blastocyst maturation, possibly via specific regulation of mRNA translation, and distinct from mechanosensory mechanisms linked to cavity expansion.

Conclusions

We have reported that p38-MAPKi during mouse blastocyst maturation (E3.5–E4.5) robustly impairs PrE specification/differentiation and is associated with significantly reduced blastocyst cavity expansion (Bora et al., 2019; 2021b; Thamodaran & Bruce, 2016); recapitulated here in Figures S1 and S2. This cavity-expansion defect resembles data showing that experimentally induced cavity volume defects lead to decreased expression of ICM fate marker proteins (EPI SOX2; PrE GATA4; Ryan et al., 2019). We sought to determine if p38-MAPKi-mediated PrE phenotypes could be reproduced by OA-induced cavity-volume impairments or whether they arise from autonomous ICM mechanisms. In agreement with the previous report (Ryan et al., 2019), OA-related cavity defects (Figure 1) correlate with reduced IF levels of specific EPI and PrE markers (Figures S5 and S7); moreover, expanding these findings shows an associated impairment in specification of overall EPI rather than PrE cell populations, in a manner consistent with a developmental delayed rather than a block (Figures 2 and3 and Figures S3, S4, and S6). These contrasting results indicate that while cavity expansion is impaired after p38-MAPKi, it is not the primary reason for the observed PrE deficit; instead, p38-MAPKi sensitivity involves ICM-autonomous mechanisms, as supported by observations in cultured IS-isolated ICMs (Figure 4 and Figure S12) and in both 2D and 3D mouse ES-cell/organoid ICM-related models (Figure 5 and Figures S13–S18). Thus, active p38-MAPK functions during early mouse blastocyst maturation to facilitate PrE specification/differentiation from uncommitted ICM progenitors as an intrinsic property of ICM cells, presumably responding to spatial–temporal cues that remain to be defined, culminating in the appropriate formation of the late-stage (E4.5) blastocyst.

Supplementary material

Supplementary material is available at *Reproduction* online.

Conflicts of interest

None declared.

Funding

This work was supported by grants from the Czech Science Foundation (GAČR, 21-03305S, awarded to A.W.B.) and the Grant Agency of the University of South Bohemia [GAJU, 027/2021/P, awarded to M.B.(S.)]. Research in the S.M.-D. group was funded by ACIISI (CEI2019-02), the ULPGC Research Support Programme, and ACIISI co-funded by FEDER Funds (ProID2020010013). J.L.-G. received support from the ULPGC predoctoral programme, and S.M.-D. was supported by the "Viera y Clavijo" Programme from the Agencia Canaria de Investigación, Innovación y Sociedad de la Información (ACIISI) and ULPGC.

Acknowledgements

We acknowledge the Institute of Parasitology (Biology Centre of the Czech Academy of Sciences, in České Budějovice) for housing mice, Marta Gajewska (Institute of Oncology, Warsaw, Poland), and Anna Piliszek (Institute of Genetics and Animal Breeding, Polish Academy of Sciences, Jastrzębiec, Poland) for founder CBA/W mice, and other laboratory members for valuable inputs and discussions. Imaging was carried out at the SIMACE (Advanced Confocal and Electron Microscopy Research Service) at the IUIBS.

Data availability statement

The data underlying this article are available in the article and in its online supplementary material and/or by personal request to the corresponding author.

References

Artus, J., Piliszek, A., & Hadjantonakis, A. K. (2011). The primitive endoderm lineage of the mouse blastocyst: sequential transcription factor activation and regulation of differentiation by Sox17. *Developmental Biology*, *350*, 393–404. https://doi.org/10.1016/j.ydbio.2010.12.007

Avilion, A. A., Nicolis, S. K., Pevny, L. H., Perez, L., Vivian, N., & Lovell-Badge, R. (2003). Multipotent cell lineages in early mouse development depend on SOX2 function. *Genes & Development*, *17*, 126–140. https://doi.org/10.1101/gad.224503

Bagnat, M., Cheung, I. D., Mostov, K. E., & Stainier, D. Y. (2007). Genetic control of single lumen formation in the zebrafish gut. *Nature Cell Biology*, *9*, 954–960. https://doi.org/10.1038/ncb1621

Bora, P., Gahurova, L., Hauserova, A., Stiborova, M., Collier, R., Potěšil, D., Zdráhal, Z., & Bruce, A. W. (2021a). DDX21 is a p38-MAPK-sensitive nucleolar protein necessary for mouse preimplantation embryo development and cell-fate specification. *Open Biology*, *11*, 210092. https://doi.org/10.1098/rsob.210092

Bora, P., Gahurova, L., Mašek, T., Hauserova, A., Potěšil, D., Jansova, D., Susor, A., Zdráhal, Z., Ajduk, A., Pospíšek, M., & Bruce, A. W. (2021b). p38-MAPK-mediated translation regulation during early blastocyst development is required for primitive endoderm differentiation in mice. *Communications Biology*, *4*, 788. https://doi.org/10.1038/s42003-021-02290-z

Bora, P., Thamodaran, V., Susor, A., & Bruce, A. W. (2019). p38-mitogen activated kinases mediate a developmental regulatory response to amino acid depletion and associated oxidative stress in mouse blastocyst embryos. *Frontiers in Cell and Developmental Biology*, *7*, 276. https://doi.org/10.3389/fcell.2019.00276

Bulut-Karslioglu, A., Biechele, S., Jin, H., Macrae, T. A., Hejna, M., Gertsenstein, M., Song, J. S., Ramalho-Santos, M. (2016). Nature, *540*, 119–123. https://doi.org/10.1038/nature20578

Chazaud, C., & Yamanaka, Y. (2016). Lineage specification in the mouse preimplantation embryo. *Development (Cambridge, England)*, *143*, 1063–1074. https://doi.org/10.1242/dev.128314

Chazaud, C., Yamanaka, Y., Pawson, T., & Rossant, J. (2006). Early lineage segregation between epiblast and primitive endoderm in mouse blastocysts through the Grb2-MAPK pathway. *Developmental Cell*, *10*, 615–624. https://doi.org/10.1016/j.devcel.2006.02.020

Del Llano, E., Masek, T., Gahurova, L., Pospisek, M., Koncicka, M., Jindrova, A., Jansova, D., Iyyappan, R., Roucova, K., Bruce, A. W., Kubelka, M., & Susor, A. (2020). Age-related differences in the translational landscape of mammalian oocytes. *Aging Cell*, *19*, e13231. https://doi.org/10.1111/acel.13231

Fischer, S. C., Corujo-Simon, E., Lilao-Garzon, J., Stelzer, E. H. K., & Munoz-Descalzo, S. (2020). The transition from local to global patterns governs the differentiation of mouse blastocysts. *PLoS One*, *15*, e0233030. https://doi.org/10.1371/journal.pone.0233030

Fonseca, B. D., Smith, E. M., Yelle, N., Alain, T., Bushell, M., & Pause, A. (2014). The ever-evolving role of mTOR in translation. *Seminars in Cell & Developmental Biology*, *36*, 102–112. https://doi.org/10.1016/j.semcdb.2014.09.014

Frankenberg, S., Gerbe, F., Bessonnard, S., Belville, C., Pouchin, P., Bardot, O., & Chazaud, C. (2011). Primitive endoderm differentiates via a three-step mechanism involving Nanog and RTK signaling. *Developmental Cell*, *21*, 1005–1013. https://doi.org/10.1016/j.devcel.2011.10.019

Gahurova, L., Tomankova, J., Cerna, P., Bora, P., Kubickova, M., Virnicchi, G., Kovacovicova, K., Potesil, D., Hruska, P., Zdrahal, Z., Anger, M., Susor, A., & Bruce, A. W. (2023). Spatial positioning of preimplantation mouse embryo cells is regulated by mTORC1 and m(7)G-cap-dependent translation at the 8- to 16-cell transition. *Open Biology*, *13*, 230081. https://doi.org/10.1098/rsob.230081

Iyyappan, R., Aleshkina, D., Ming, H., Dvoran, M., Kakavand, K., Jansova, D., Del Llano, E., Gahurova, L., Bruce, A. W., Masek, T., Pospisek, M., Horvat, F., Kubelka, M., Jiang, Z., & Susor, A. (2023). The translational oscillation in oocyte and early embryo development. *Nucleic Acids Research*, *51*, 12076–12091. https://doi.org/10.1093/nar/gkad996

Jackson, J. R., Bolognese, B., Hillegass, L., Kassis, S., Adams, J., Griswold, D. E., & Winkler, J. D. (1998). Pharmacological effects of SB 220025, a selective inhibitor of P38 mitogen-activated protein kinase, in angiogenesis and chronic inflammatory disease models. *The Journal of Pharmacology and Experimental Therapeutics*, *284*, 687–692.

Kalmar, T., Lim, C., Hayward, P., Munoz-Descalzo, S., Nichols, J., Garcia-Ojalvo, J., & Martinez Arias, A. (2009). Regulated fluctuations in nanog expression mediate cell fate decisions in embryonic stem cells. *PLoS Biology*, *7*, e1000149. https://doi.org/10.1371/journal.pbio.1000149

Kang, M., Piliszek, A., Artus, J., & Hadjantonakis, A. K. (2013). FGF4 is required for lineage restriction and salt-and-pepper distribution of primitive endoderm factors but not their initial expression in the mouse. *Development (Cambridge, England)*, *140*, 267–279. https://doi.org/10.1242/dev.084996

Lou, X., Kang, M., Xenopoulos, P., Munoz-Descalzo, S., & Hadjantonakis, A. K. (2014). A rapid and efficient 2D/3D nuclear segmentation method for analysis of early mouse embryo and stem cell image data. *Stem Cell Reports*, *2*, 382–397. https://doi.org/10.1016/j.stemcr.2014.01.010

Mammoto, T., Mammoto, A., & Ingber, D. E. (2013). Mechanobiology and developmental control. *Annual Review of Cell and Developmental Biology*, *29*, 27–61. https://doi.org/10.1146/annurev-cellbio-101512-122340

Manejwala, F. M., Cragoe, , E. J.Jr., & Schultz, R. M. (1989). Blastocoel expansion in the preimplantation mouse embryo: role of extracellular sodium and chloride and possible apical routes of their entry. *Developmental Biology*, *133*, 210–220. https://doi.org/10.1016/0012-1606(89)90312-6

Masek, T., Del Llano, E., Gahurova, L., Kubelka, M., Susor, A., Roucova, K., Lin, C. J., Bruce, A. W., & Pospisek, M. (2020). Identifying the translatome of mouse NEBD-stage oocytes via SSP-profiling; a novel polysome fractionation method. *International Journal of Molecular Sciences*, *21*, 1254. https://doi.org/10.3390/ijms21041254

Mathew, B., Munoz-Descalzo, S., Corujo-Simon, E., Schroter, C., Stelzer, E. H. K., & Fischer, S. C. (2019). Mouse ICM organoids reveal three-dimensional cell fate clustering. *Biophysical Journal*, *116*, 127–141. https://doi.org/10.1016/j.bpj.2018.11.011

McCloy, R. A., Rogers, S., Caldon, C. E., Lorca, T., Castro, A., & Burgess, A. (2014). Partial inhibition of Cdk1 in G 2 phase overrides the SAC and decouples mitotic events. *Cell Cycle (Georgetown, Tex.)*, *13*, 1400–1412. https://doi.org/10.4161/cc.28401

Mihajlovic, A. I., & Bruce, A. W. (2016). Rho-associated protein kinase regulates subcellular localisation of Angiomotin and Hippo-signalling during preimplantation mouse embryo development. *Reprod Biomed Online*, *33*, 381–390.

Mihajlovic, A. I., Thamodaran, V., & Bruce, A. W. (2015). The first two cell-fate decisions of preimplantation mouse embryo development are not functionally independent. *Sci Rep*, *5*, 15034.

Motosugi, N., Bauer, T., Polanski, Z., Solter, D., & Hiiragi, T. (2005). Polarity of the mouse embryo is established at blastocyst and is not prepatterned. *Genes & Development*, *19*, 1081–1092. https://doi.org/10.1101/gad.1304805

Niakan, K. K., Ji, H., Maehr, R., Vokes, S. A., Rodolfa, K. T., Sherwood, R. I., Yamaki, M., Dimos, J. T., Chen, A. E., Melton, D. A., McMahon, A. P., & Eggan, K. (2010). Sox17 promotes differentiation in mouse embryonic stem cells by directly regulating extraembryonic gene expression and indirectly antagonizing self-renewal. *Genes & Development*, *24*, 312–326. https://doi.org/10.1101/gad.1833510

Nichols, J., Silva, J., Roode, M., & Smith, A. (2009). Suppression of Erk signalling promotes ground state pluripotency in the mouse embryo. *Development (Cambridge, England)*, *136*, 3215–3222. https://doi.org/10.1242/dev.038893

Ozadam, H., Tonn, T., Han, C. M., Segura, A., Hoskins, I., Rao, S., Ghatpande, V., Tran, D., Catoe, D., Salit, M., & Cenik, C. (2023). Single-cell quantification of ribosome occupancy in early mouse development. *Nature*, *618*, 1057–1064. https://doi.org/10.1038/s41586-023-06228-9

Plusa, B., & Piliszek, A. (2020). Common principles of early mammalian embryo self-organisation. *Development*, *147*, dev183079.

Posfai, E., Petropoulos, S., de Barros, F. R. O., Schell, J. P., Jurisica, I., Sandberg, R., Lanner, F., & Rossant, J. (2017). Position- and Hippo signaling-dependent plasticity during lineage segregation in the early mouse embryo. *eLife*, *6,* e22906. https://doi.org/10.7554/eLife.22906

Potapova, T. A., Sivakumar, S., Flynn, J. N., Li, R., & Gorbsky, G. J. (2011). Mitotic progression becomes irreversible in prometaphase and collapses when Wee1 and Cdc25 are inhibited. *Molecular Biology of the Cell*, *22*, 1191–1206. https://doi.org/10.1091/mbc.E10-07-0599

Ryan, A. Q., Chan, C. J., Graner, F., & Hiiragi, T. (2019). Lumen expansion facilitates epiblast-primitive endoderm fate specification during mouse blastocyst formation. *Developmental Cell*, *51*, 684–697 e684. https://doi.org/10.1016/j.devcel.2019.10.011

Schindelin, J., Arganda-Carreras, I., Frise, E., Kaynig, V., Longair, M., Pietzsch, T., Preibisch, S., Rueden, C., Saalfeld, S., Schmid, B., Tinevez, J.-Y., White, D. J., Hartenstein, V., Eliceiri, K., Tomancak, P., & Cardona, A. (2012). Fiji: an open-source platform for biological-image analysis. *Nature Methods*, *9*, 676–682. https://doi.org/10.1038/nmeth.2019

Schliffka, M. F., Dumortier, J. G., Pelzer, D., Mukherjee, A., & Maître, J.-L. (2024). Inverse blebs operate as hydraulic pumps during mouse blastocyst formation, *Nat Cell Biol*, *26(10)*, 1669–1677. https://doi.org/10.1038/s41556-024-01501-z.

Schroter, C., Rue, P., Mackenzie, J. P., & Martinez Arias, A. (2015). FGF/MAPK signaling sets the switching threshold of a bistable circuit controlling cell fate decisions in embryonic stem cells. *Development*, *142*, 4205–4216.

Solter, D., & Knowles, B. B. (1975). Immunosurgery of mouse blastocyst. *Proceedings of the National Academy of Sciences of the United States of America*, *72*, 5099–5102. https://doi.org/10.1073/pnas.72.12.5099

Thamodaran, V., & Bruce, A. W. (2016). p38 (Mapk14/11) occupies a regulatory node governing entry into primitive endoderm differentiation during preimplantation mouse embryo development. *Open Biology*, *6*, 16019. https://doi.org/10.1098/rsob.160190

Watson, A. J. (1992). The cell biology of blastocyst development. *Molecular Reproduction and Development*, *33*, 492–504. https://doi.org/10.1002/mrd.1080330417

Watson, A. J., & Barcroft, L. C. (2001). Regulation of blastocyst formation. *Frontiers in Bioscience: a Journal and Virtual Library*, *6*, D708–730. https://doi.org/10.2741/watson

Wicklow, E., Blij, S., Frum, T., Hirate, Y., Lang, R. A., Sasaki, H., & Ralston, A. (2014). HIPPO pathway members restrict SOX2 to the inner cell mass where it promotes ICM fates in the mouse blas-

tocyst. *PLoS Genetics*, *10*, e1004618. https://doi.org/10.1371/journal.pgen.1004618

Wigger, M., Kisielewska, K., Filimonow, K., Plusa, B., Maleszewski, M., & Suwińska, A. (2017). Plasticity of the inner cell mass in mouse blastocyst is restricted by the activity of FGF/MAPK pathway. *Scientific Reports*, *7*, 15136. https://doi.org/10.1038/s41598-017-15427-0

Wiley, L. M. (1984). Cavitation in the mouse preimplantation embryo: Na/K-ATPase and the origin of nascent blastocoele fluid. *Developmental Biology*, *105*, 330–342. https://doi.org/10.1016/0012-1606(84)90290-2

Yamanaka, Y., Lanner, F., & Rossant, J. (2010). FGF signal-dependent segregation of primitive endoderm and epiblast in the mouse blastocyst. *Development (Cambridge, England)*, *137*, 715–724. https://doi.org/10.1242/dev.043471